Available online at www.sciencedirect.com
SCIENCE DIRECT®
Journal of Power Sources 132 (2004) 42–51
JOURNAL OF POWER SOURCES
www.elsevier.com/locate/jpowsour

Numerical simulation of a disk-type SOFC for impedance analysis under power generation

Kiyonami Takano [a,*], Susumu Nagata [a], Ken Nozaki [a], Akihiko Monma [a], Tohru Kato [a], Yasuo Kaga [a], Akira Negishi [a], Ken Kato [a], Toru Inagaki [b], Hiroyuki Yoshida [b], Kei Hosoi [c], Koji Hoshino [c], Taner Akbay [c], Jun Akikusa [c]

[a] *Fuel Cell Group, Energy Electronics Institute, AIST, 1-1-1 Umezono Tsukuba-shi, Ibaraki 305-8568, Japan*
[b] *Technical Research Center, The Kansai Electric Power Company, Inc., 11-20 Nakoji, 3-Chome, Amagasaki, Hyogo 661-0974, Japan*
[c] *Central Research Institute, Naka Research Center, Mitsubishi Materials Corp., 1002-14 Mukohyama, Naka-machi, Naka-gun, Ibaraki 311-0102, Japan*

Received 17 September 2003; received in revised form 14 January 2004; accepted 16 January 2004

Abstract

To support the impedance analysis in a disk-type SOFC under power generation, a numerical simulation procedure, whose simulation outputs the total impedance of an actual-size disk-type SOFC cell for the input of the local impedance of cell, has been proposed. In the simulation, the quasi-one-dimensional radial flow and mass transport problem with cell reactions is solved. Transient distributions of electromotive force, current and concentrations of chemical species in the cell are calculated to obtain the total cell impedance with parameters, such as local impedance of the cell, ac frequency, fuel utilization, gas flow rate, etc. A parametric simulation study for the simplest case under typical experimental conditions has been carried out. It is found that the Cole–Cole plot for the total cell impedance shows a capacitive semicircle, even if a pure resistance is assumed as the local impedance of the cell. The diameter of the impedance semicircle changes with fuel utilization and supplied gas flow rate, being affected by the diffusion in the flow direction. The characteristic frequency of the impedance semicircle depends on the transit time of the gas through the cell which is also affected by the diffusion in the flow direction. It is also suggested that the total cell impedance appears as a convolution of this capacitive semicircle impedance and local impedance of the cell.

Keywords: Disk-type SOFC; Numerical simulation; Impedance analysis; Power generation; Gas conversion impedance

1. Introduction

The ac impedance analysis is one of the most effective methods not only for characterization of materials and electrodes in electrochemical systems, but also for obtaining characteristic data necessary for system design and simulations. The equivalent circuit obtained from the impedance analysis would be especially useful for the simulation of the dynamic performance of such systems. Various types of solid oxide fuel cells have been under development in the USA, Europe and Japan, and the concept is already in the demonstration stage for commercialization at Siemens Westinghouse Power Corporation [1], Sulzer Hexis, Ltd. [2], etc. However, impedance analyses of commercial size SOFCs under practical power generation conditions have been scarcely reported [3,4]. The main reason for this is that the measurement and the interpretation of impedance in a full-scale cell is rather difficult, due to the nonuniform current distribution in the cell and the unknown correlation between the local impedance of the cell and the total cell impedance.

Disk-type SOFCs have currently been developed by Sulzer Hexis, Ltd. [2] and Mitsubishi Materials Corporation in collaboration with the Kansai Electric Power Company, Inc. [5,6]. In a disk-type axially symmetric cell (e.g. Mitsubishi Materials type), the impedance measurement and analysis may be greatly simplified [6].

Many experimental investigations on impedance of the SOFC cell have been conducted using small-size cells [2,7–12]. Generally, the impedance of the SOFC cell is related with many factors, such as ionic and electronic conductivities, diffusivities of the chemical species in the electrolyte and electrodes, reaction activation over-potentials at the anode and cathode, and diffusion of the chemical

* Corresponding author. Tel.: +81-298-61-5794; fax: +81-298-61-5805.
E-mail address: k.takano@aist.go.jp (K. Takano).

0378-7753/$ – see front matter © 2004 Elsevier B.V. All rights reserved.
doi:10.1016/j.jpowsour.2004.01.038

Nomenclature

c	molar density (mol/cm^3)
C_d	double layer capacity per unit area (F/cm^2)
C_g	parallel capacity for gas conversion impedance (F)
C_{wg}	normalized parallel capacity for whole-cell gas-conversion impedance (F/cm^2)
D	diffusion coefficient (cm^2/s)
D_{cell}	cell diameter (cm)
E_{emf}	electromotive force (V)
F	Faraday constant (C/mol)
$\Delta G^{\circ}_{H_2O}$	Gibbs free energy change in the reaction $H_2 + \frac{1}{2}O_2 \rightleftarrows H_2O$ at the standard pressure (0.1 MPa) and reference state (J/mol)
h	channel effective height (cm)
I_L	load current (A)
J_r	current density for reaction (A/cm^2)
N	volumetric flow rate (cm^3/s)
p	total pressure or partial pressure (0.1 MPa)
r	radius (cm)
R	gas constant (J/mol/K)
R_{cell}	local cell resistance per unit area (Ω cm^2)
R_e	electronic resistance per unit area (Ω cm^2)
R_i	ionic resistance per unit area (Ω cm^2)
R_g	parallel resistance for gas conversion impedance (Ω)
R_r	reaction resistance per unit area (Ω cm^2)
R_s	serial Ohmic resistance per unit area (Ω cm^2)
R_{wg}	normalized parallel resistance for whole-cell gas-conversion impedance (Ω cm^2)
τ_{wg}	time constant for whole-cell gas-conversion impedance (s)
τ_d	time constant for diffusion in z-direction, D/h^2 (s)
t	time (s)
T	temperature (K)
U_f	fuel utilization
U_{eff}	effective fuel utilization
v	molar average flow velocity (cm/s)
V	controlled volume by electrode reaction (cm^3)
V_{ac}	amplitude of ac voltage (V)
V_{dc}	dc voltage (V)
V_{cell}	cell terminal voltage (V)

Subscripts

a	air
f	fuel
H_2	hydrogen
H_2O	water vapor
M	H_2, H_2O or O_2
O_2	oxygen
r	radial axis direction
z	z-axis direction

species in the gas flow channel. It also depends on the cell construction and working conditions. If the basic cell design, such as the sizes, materials and structures of the electrolyte and electrodes and the morphologies of their interfaces is given, the impedance may be a function of the working conditions, such as temperature, pressure and the compositions of the fuel and oxidizing agent.

This study deals with a simulation method which links the local impedance of the cell with the total cell impedance at the power generation under the assumption that the local impedance is given by a function of the frequency with some parameters, such as temperature, total pressure and the compositions of fuel and oxidizing agent. In this study, a numerical simulation procedure has been proposed in order to support the impedance analysis in a disk-type commercial size SOFC under power generation. In the simulation, a quasi-one-dimensional radial flow and mass transport problem including cell reactions was numerically solved as a function of voltage and direct current superimposed with a small alternating current. With a given function of the local impedance, transient distributions of the current, electromotive force and concentrations of chemical species in the cell were calculated, and the total output current as a function of time was obtained. Thus, the total cell impedance was calculated by using the Fourier transforms. A parametric simulation study for the simplest case under typical experimental conditions was also carried out by changing parameters, such as applied ac frequency, load currents (fuel utilization), cell dimensions, supplied gas flow rates and the local impedance of the cell, and the results are discussed.

2. Simulation model

2.1. Model assumptions and discussions

The schematic diagram of a disk-type SOFC as a simulation model is shown in Fig. 1. The single cell consists of a composite disk made of a solid electrolyte with electrodes on both sides, structured current collectors and metal separators for positive and negative electrodes. Hydrogen as fuel and air as oxidant are supplied through orifices located

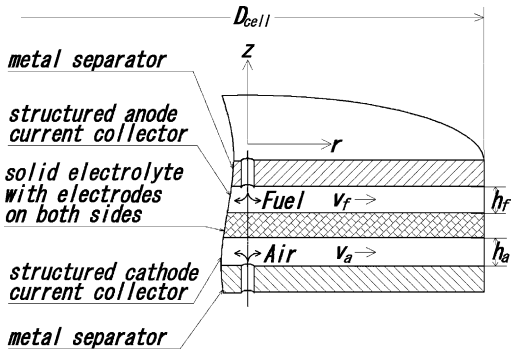

Fig. 1. Schematic diagram of a disk-type SOFC.

at the center of each separator, and the structured current collectors aided the uniformly distributed axially symmetric gas flow. It is assumed that the solid electrolyte and electrodes and the current collectors are homogeneous with uniform thicknesses. Although cell reactions take place on the electrolyte surface, it is assumed that the concentrations of the chemical species are constant along the z direction due to perfect mixing by diffusion. This assumption is valid for the transient behaviors with the characteristic time constant larger than the diffusion time constant $\tau_d = D/h^2$, if the parameter $\mathfrak{R} \equiv v_{ro}h^2/r_o D$ which is a rough ratio of the radial flow convection term and the z-direction diffusion term in the molar transport equation is sufficiently small, where v_{ro} is the radial flow velocity at the cell outlet, r_o the cell outer radius, h the height of the gas flow channel, and D the diffusion coefficient. The precise discussion about this parameter is given in the appendix. It is also assumed that the pressure drop in the channel is small. Therefore, the total pressure is constant. For further simplicity, the temperature is assumed to be uniform in the cell in this paper, though it should be determined by solving the heat transfer problem in the cell in a future work. This assumption can be approximately realized by externally heating the separators during the experiment.

The conductivity of the current collector is sufficiently large, hence, the cell potential, V_{cell} between the cathode and anode, is constant everywhere in the collectors. The thicknesses of the electrodes and electrolyte are sufficiently thin relative to their areas, and the currents in the r-direction are much smaller than the total current. Therefore, it is assumed that the reaction current density and the output current density are locally determined by the local impedance with the local electromotive force and the cell voltage.

2.2. Governing equations

Basic equations governing the system are as follows:

The electromotive force E_{emf} can be obtained from

$$E_{emf} = -\frac{\Delta G^{\circ}_{H_2O}}{2F} + \frac{RT}{2F}\ln\frac{p_{H_2}p_{O_2}^{0.5}}{p_{H_2O}} \tag{1}$$

where $\Delta G^{\circ}_{H_2O}$ is the Gibbs free energy change in the reaction $H_2 + \frac{1}{2}O_2 \rightleftarrows H_2O$ at the standard pressure and reference state, F the Faraday's constant, R the gas constant, T the temperature, p_{H_2} the hydrogen partial pressure, p_{O_2} the oxygen partial pressure, p_{H_2O} the water partial pressure.

The cell voltage V_{cell} is given by

$$V_{cell} = V_{dc} + V_{ac}\sin(2\pi f t) \tag{2}$$

where V_{dc} is the dc cell voltage, V_{ac} the amplitude of applied ac voltage, f the frequency, t the time.

Transport equations for the molar densities of hydrogen, water and oxygen considering the diffusion in the flow direction are

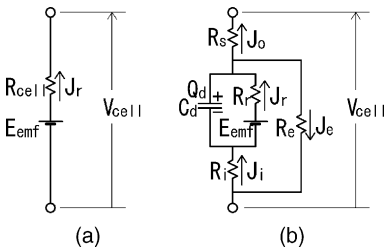

Fig. 2. Equivalent circuits for local cell in SOFC: (a) simplest circuit; (b) considering reaction resistance with double layer and electronic conduction in solid electrolyte.

$$\frac{\partial c_{H_2}}{\partial t} + \frac{1}{r}\frac{\partial}{\partial r}r\left(v_f c_{H_2} - D_{H_2}\frac{\partial c_{H_2}}{\partial r}\right) = -\frac{J_r}{2Fh_f} \tag{3}$$

$$\frac{\partial c_{H_2O}}{\partial t} + \frac{1}{r}\frac{\partial}{\partial r}r\left(v_f c_{H_2O} - D_{H_2O}\frac{\partial c_{H_2O}}{\partial r}\right) = \frac{J_r}{2Fh_f} \tag{4}$$

$$\frac{\partial c_{O_2}}{\partial t} + \frac{1}{r}\frac{\partial}{\partial r}r\left(v_a c_{O_2} - D_{O_2}\frac{\partial c_{O_2}}{\partial r}\right) = -\frac{J_r}{4Fh_a} \tag{5}$$

where c is the molar density, v the molar average flow velocity, D the diffusion coefficient, r the radius, J_r the cell reaction current density, h the effective channel height. Subscripts: H_2, H_2O, O_2, f, a the hydrogen, water, oxygen, fuel, air, respectively. The cell reaction current density J_r is locally calculated by E_{emf} and V_{cell} from the given function of the local impedance as well as the output current density J_0, as previously mentioned. For the simplest example, the local impedance consists of a pure resistance R_{cell} as shown in Fig. 2a, J_r and J_0 are given by

$$J_r = J_0 = \frac{E_{emf} - V_{cell}}{R_{cell}} \tag{6}$$

Furthermore, the continuity may be described as

$$\frac{1}{r}\frac{\partial}{\partial r}rv_f = 0 \tag{7}$$

$$\frac{1}{r}\frac{\partial}{\partial r}rv_a = -\frac{RT}{p}\frac{J_r}{4Fh_a} \tag{8}$$

where p is the total pressure. Finally, the relationship between the partial pressure p_M and the molar density c_M of the chemical species M is given as follows:

$$p_M = c_M RT \tag{9}$$

2.3. Local impedance of cell

The function of the local impedance is easily obtained, if the impedance can be expressed by an equivalent circuit. According to the impedance analysis of SOFC, the impedance changes with frequency between several MHz and sub mHz, and it has been expressed by the equivalent circuits of the combination of resistive elements and capacitive elements, inductivity elements, etc. [6–12]. In this paper, the impedance of the frequency range below 100 Hz is

monitored, where the impedance may be affected by the gas flow.

To examine the effect of the gas flow, the simplest equivalent circuit consisting of a constant pure resistance as shown in Fig. 2a is used as the local impedance. Furthermore, the solid electrolyte has electronic conductance as well as ionic conductance. Thus, in order to examine the effect of the mixed conductivity in the electrolyte as well as the complex local impedance, an equivalent circuit as shown in Fig. 2b, which includes a representative RC parallel circuit with reaction resistance R_r and double layer capacitance C_d, electronic resistance R_e, ionic resistance R_i and series ohmic resistance R_S is also used for comparison and discussion.

2.4. Numerical method and conditions in calculation

The previously described partial differential equations were numerically solved by employing the implicit finite difference method. For the simplification of the calculation, the diffusion was assumed to be zero at the inlet and the outlet of the channels as boundary conditions. This condition could be experimentally justified. If the port for supplying the gas at the inlet is small enough to have high speed, and the channels are narrow enough and long enough without electrodes at the downstream of the cell reaction regions, the resulting convection molar flux is much greater than the diffusion molar flux. The stationary solution for the direct current case was calculated by assuming the open-circuit as an initial condition. The result was then used as an initial condition for the case where the ac current superimposed on the dc current. The load current I_L was calculated by integrating the output current density J_0 over the entire cell area as a function of time. The Fourier transforms of the load current and the applied ac voltage were used to calculate the total cell impedance.

The calculation conditions of the reference case and the parametric study are shown in Table 1. These conditions were based on the experimental setup for the impedance measurements at Mitsubishi Materials Corporation [6]. Additional parameters are dc voltage, load current and fuel utilization. Because these parameters are not independent, the fuel utilization factor U_f defined below will be mainly used as follows:

$$U_f = \frac{I_L}{2Fm_{H_2}} \tag{10}$$

where I_L the load current, m_{H_2} molar flow rate of the supplied hydrogen. The calculation was carried out with an applied ac voltage of 1 mV amplitude for a range of frequencies between 100 and 0.01 Hz. The cell was meshed with 100 elements, and time step Δt was chosen between 0.1 and 5 ms depending on the frequency. The diffusion coefficient was evaluated by the Chapman and Enskog equation as a function of temperature and pressure [13].

Table 1
Simulation conditions

Parameter	Reference case	Parametric study
Cell diameter D_{cell} (cm)	8.5	17
Channel effective height (cm)		
h_f	0.1	0.05
h_a	0.1	0.05
Fuel flow rate G_f (Ncc/min/cm^2)	3	6
Air flow rate G_a (Ncc/min/cm^2)	15	30
Temperature T (K)	1023.15	973.15
Total pressure p (MPa)	0.1013	0.2026
Fuel utilization U_f (%)	80	10–90
Local cell impedance R_{cell} (Ω cm^2)	0.5	Table 2
Diffusion coefficient (cm^2/s)		
D_f	7.06	0, 6.48[a], 3.53[b]
D_a	1.65	0, 1.52[a], 0.825[b]
Inlet H_2O mole fraction in fuel (%)	1	1
Inlet H_2 mole fraction in fuel (%)	99	99
Inlet O_2 mole fraction in air (%)	20.95	20.95
Inlet N_2 mole fraction in air (%)	79.05	79.05

[a] For 973.15 K at 0.1013 MPa.
[b] For 1023.15 K at 0.2026 MPa.

Here, the Peclet number, $P_e = vL/D$ (v: velocity, L the characteristic length; D the diffusion coefficient), which is defined as the ratio of the convection flux and the diffusion flux, is estimated to be about 2.4 for the radial fuel flow and about 50 for the radial air flow, by taking the cell outer radius r_o ($r_o = 4.25$ cm) as the characteristic length and the outlet velocity v_{ro} ($v_{ro} \approx 4$ cm/s for fuel flow and $v_{ro} \approx 20$ cm/s for air flow at the reference case) as the velocity. This means that the convections are dominant in the r-direction, and the r-direction diffusion in the fuel channel is not negligible. For the Peclet number in the z-direction, $P_e = 0$ for the fuel flow channel because there is no total molar flow in the z-direction in the fuel channel, and $P_e \leq 0.013$ for the air flow channel with the cell reaction of 1 A/cm^2 ($v_z = 0.22$ cm/s, which is caused by the consumption of O_2 at the electrode surface). That is, the diffusion is much larger than the convection in the z-direction. Further more, the parameter $\Re = v_{ro}h^2/r_oD$ is estimated to be $\Re \approx 1.3 \times 10^{-3}$ for the fuel flow channel and $\Re \approx 2.9 \times 10^{-2}$ for the air flow channel. This means that the lateral change in the mole fraction is much smaller than the longitudinal change at steady state. The parameter τ_d for the diffusion characteristic time in the z direction is estimated to be $\tau_d = 1.4 \times 10^{-3}$ s for the fuel flow channel and $\tau_d = 6.1 \times 10^{-3}$ s for the air flow channel. Thus, these estimations support the assumption that the perfect mixing in the z-direction is valid for the impedance simulation at the frequency below 26 Hz ($1/(2\pi\tau_d)$). If the impedance due to gas diffusion in the z-direction at frequencies higher than $1/(2\pi\tau_d)$ is important, such impedance can be considered as a component of the local impedance as well as the impedances for the finite rate reaction, etc.

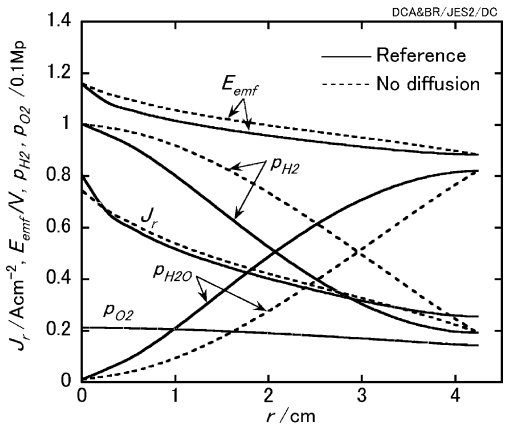

Fig. 3. Radial distributions of electromotive force, current density, and partial pressures of H_2, H_2O and O_2 under the reference conditions. Solid line: with diffusion, broken line: without diffusion.

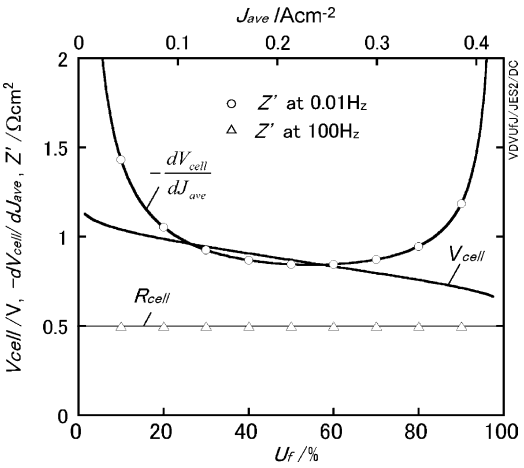

Fig. 4. Variations of cell voltage V_{cell} differential cell resistance dV_{cell}/dJ_{ave} and real parts of calculated total cell impedance at 100 and 0.01 Hz with fuel utilization for the reference conditions.

3. Results and discussion

3.1. Voltage–current characteristics and differential resistance

The steady-state distributions of the electromotive force, current density and partial pressures of chemical species for the fuel utilization of 80% under the reference conditions are shown in Fig. 3. Due to the current flow dictated by the cell reaction, partial pressure values of the hydrogen and oxygen decrease, while the steam partial pressure increases with the gas flow. As a result, the electromotive force and the current density decrease in the radial direction. The results obtained by neglecting the diffusion under the reference conditions are also shown in Fig. 3. By comparing the two cases, it is noticeable that the increase in water vapor along the flow direction is promoted by the diffusion making the water partial pressure higher and the hydrogen partial pressure lower in the upper-stream region. Thus, the drop in the electromotive force becomes larger along the flow direction, and the cell voltage decreases inevitably in order to output the demanded value of the total current (fuel utilization). In other words, the cell performance gets lowered by the existence of diffusion.

Under the reference conditions, the relationships between the cell voltage and the fuel utilization (or the load current density) and the derivative of the cell voltage with respect to the current density are shown in Fig. 4. The cell voltage decreases with current density, and the change in the cell voltage becomes greater as the fuel utilization approaches zero or 100%. This occurs because the dependence of the electromotive force to partial pressures becomes greater as the fuel utilization approaches zero or 100%. The derivative of the cell voltage with respect to the current density has the dimension of resistance per unit area, and it will be henceforth referred to as the differential cell resistance.

3.2. impedance

The variations of the calculated whole-cell impedance versus the fuel utilization for frequencies between 100 and 0.01 Hz under the reference conditions are shown as Cole–Cole plots in Fig. 5. It is very interesting to note that the Cole–Cole plots depict perfect semicircles despite the assumption of a pure resistance as local impedance of the cell. This describes the change in electromotive force due to the cell current through the change in the reactant concentration by the cell reaction. The impedance with the same mechanism in an ideal cell with a small volume has already been reported as gas conversion impedance by Primdahl and Mogensen [14]. By assuming a perfect mixing in the gas related to the anode reaction, they analyzed the change in the electromotive force caused by the gas conversion due to the cell reaction in the anode and analytically derived

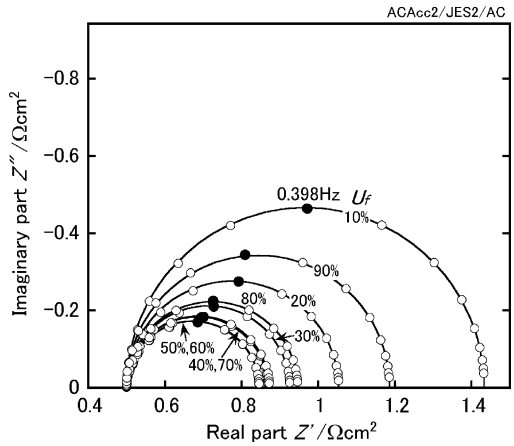

Fig. 5. Impedance Cole–Cole plots between 0.01 and 100 Hz with parameter of fuel utilization under the reference conditions. Open and closed symbols: simulation results; Solid line: fitting by an equivalent circuit with an RC parallel circuit as shown in Fig. 7a. Closed symbol shows the point of the frequency value noted in the figure.

an expression for the gas conversion impedance as an RC parallel circuit. The ideal cell with perfect mixing should be sufficiently small with enough diffusion, and it is just an entrance element of the segmented cell in our simulation. The impedance of the whole cell cannot be obtained by a simple integration over the grid. Therefore, the simulation is an effective method to obtain the total cell impedance.

For the simulation results shown in Fig. 5, the high-frequency edge of the semicircle does not change even by changing the fuel utilization. However, the diameter of the semicircle changes with the fuel utilization, and it becomes bigger as the fuel utilization approaches either zero or 100%, having a minimum value at the fuel utilization of about 50–60%.

Such impedance characteristics can be explained as follows: When the applied alternating current has a frequency enough higher than the transit time of the gas through the cell, the concentration-change of the chemical species by the applied alternating current becomes nearly zero, because it is proportional to the integrated value of the reaction quantity in a half cycle. Any change in the electromotive force does not occur if the partial pressures of the chemical species remain constant. Thus, the total cell impedance agrees with the integrated local impedance. On the other hand, for the applied alternating current with low frequency which can be considered as a small change in the direct current, the impedance agrees with the previously mentioned differential resistance of dc, *V–I* characteristics. This fact is indicated as the simulation result in Fig. 4, in which the real parts of the impedances at the high-frequency edge and at the low-frequency edge are shown, as well as the local cell resistance and the differential resistance. Therefore, the size of the semicircle changes with the fuel utilization according to the change in the differential cell resistance.

Fig. 5 also shows the fitted curves superimposed onto the simulation results using the RC parallel circuit. It is very interesting to notice that the whole-cell gas conversion impedance of a large-size cell can also be successfully expressed by an RC parallel circuit used for a small-size ideal cell.

According to Primdahl and Mogensen [14], the frequency (that will be henceforth referred to as the characteristic frequency) for which the imaginary part of impedance has a maximum value, f_g is given by

$$f_g = \frac{N}{2\pi V} \tag{11}$$

where N the fuel volume flow rate, V the separate volume related with the anode reaction. The equation dictates that the characteristic frequency is determined from the period in which the volume V of the gas is replaced by the flow, that is, the transit time of gas through the cell. Regarding the reference conditions, the period calculated by using the volume of the fuel channel as V is 0.53 s, and the characteristic frequency is 0.3 Hz. This value is about the same order of magnitude but lower than the characteristic frequency in the simulation results depicted in Fig. 5. The reason for this seems to be as follows: There is a similar phenomenon in the cathode reaction as the gas conversion in the anode reaction, and the characteristic frequency for the cathode is estimated to be 1.5 Hz for the air flow channel. The simulation results in Fig. 5 are convolutions of two phenomena for the anode and cathode. Here it should be remarked that the influence on the impedance of the cathode phenomenon is relatively small because the change in the oxygen partial pressure in the air flow channel due to the cell current is small, and the electromotive force change is small. Fig. 6 shows the simulation result for the case without diffusion under the reference conditions. This indicates that the diffusion in the radial direction causes the characteristic frequency to be lower.

The expressions of the gas conversion impedance given by Primdahl and Mogensen [14] are

$$R_g = \left(\frac{RT}{2F}\right)^2 \left(\frac{1}{p_{H_2O}} + \frac{1}{p_{H_2}}\right) \frac{1}{N} \tag{12}$$

$$C_g = \left(\frac{2F}{RT}\right)^2 \frac{1}{1/p_{H_2O} + 1/p_{H_2}} V \tag{13}$$

where, R_g and C_g are the resistance and the capacitance of a parallel circuit for the gas conversion impedance, respectively. These equations are valid for the qualitative discussions of the effect of various parameters on the impedance behaviors of the cells in large scale as will be mentioned in the following section. However, in the practical loaded conditions, they cannot be applied for the evaluations of the impedance of the large cells where the concentrations of gaseous species are distributed and have no specific values.

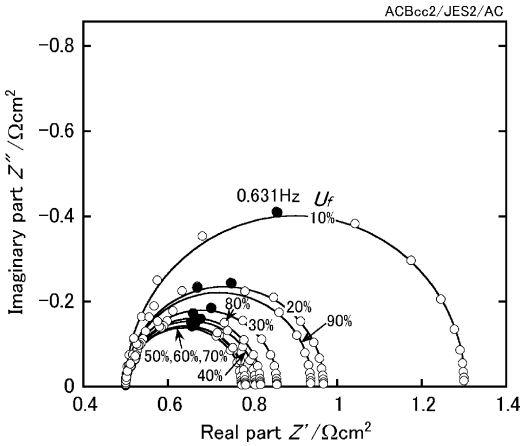

Fig. 6. Impedance Cole–Cole plots between 0.01 and 100 Hz with parameter of fuel utilization for the reference conditions without diffusion. Open and closed symbols: simulation results; Solid line: fitting by an equivalent circuit with an RC parallel circuit as shown in Fig. 7a. Closed symbol shows the point of the frequency value noted in the figure.

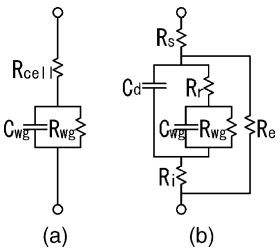

Fig. 7. Equivalent circuit for the whole-cell impedance considering the gas-conversion impedance by an RC parallel circuit with R_{wg} and C_{wg}.

3.3. Influence of design parameters on total cell impedance

The influence of various design parameters, such as cell dimensions and operating conditions, on the total cell impedance was parametrically examined. Parameter fitting was performed for the simulation results by the impedance equivalent circuit depicted in Fig. 7. This equivalent circuit for the alternating current was derived from the SOFC equivalent circuit of Fig. 2 by substituting an RC parallel circuit with R_{wg} and C_{wg} for the electromotive force. In addition, the total cell impedance was normalized by the cell area. The error in each fitting was sufficiently small as well as in Figs. 5 and 6, and it was confirmed that the impedance on the high-frequency edge agreed with the local cell resistance in each case.

Figs. 8 and 9 show R_{wg} and the time constant of $\tau_{wg} = R_{wg}C_{wg}$ for the whole-cell gas-conversion impedance for the reference case and for the cases, such as neglected diffusion, double gas flow rate, half channel height, double cell diameter, temperatures lowered to 973 K, or pressure doubled under the reference conditions.

The influence of most of the parameters on the whole-cell gas-conversion impedance can be explained in principle via Eqs. (11) and (12).

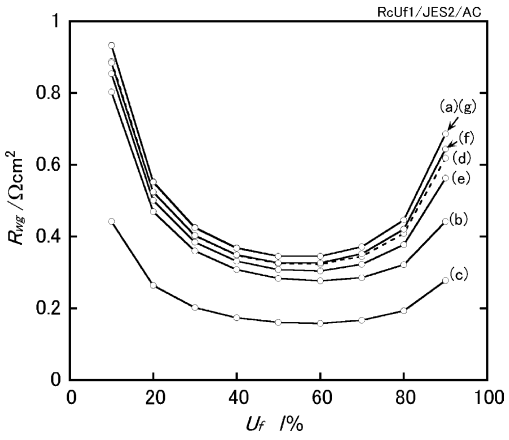

Fig. 8. R_{wg} vs. fuel utilization with changing parameter: (a) reference case; (b) neglected diffusion; (c) doubled gas flow rates; (d) halved channel heights; (e) doubled cell diameter; (f) 973 K temperature and (g) doubled total pressure.

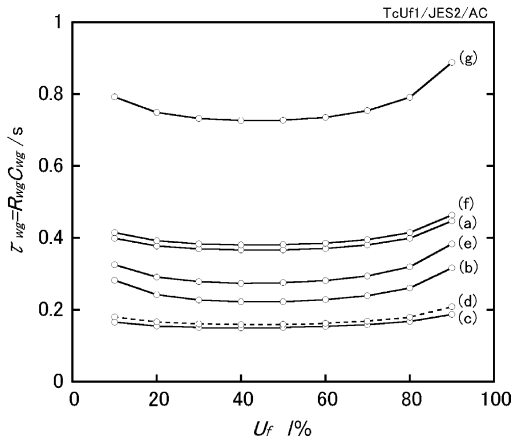

Fig. 9. τ_{wg} vs. fuel utilization with changing parameter: (a) reference case; (b) neglected diffusion; (c) doubled gas flow rates; (d) halved channel heights; (e) doubled cell diameter; (f) 973 K temperature and (g) doubled total pressure.

For all cases in Fig. 8, normalized resistance R_{wg} is a function of the fuel utilization and becomes bigger as the fuel utilization approaches either 0 or 100%, having a minimum value at the fuel utilization around 50–60%. This may be guessed from Eq. (12) by considering the dependence of R_g on the partial pressures of hydrogen and water vapor. As shown in Fig. 9, the time constant τ_{wg} scarcely changes with the fuel utilization between 20 and 80%, but considerably increases as the fuel utilization approaches zero or 100%, although the transit time of the gas does not change. Such behavior cannot be simply explained, but it qualitatively agrees with the experimental results [6]. It seems to be related to the distribution of the chemical species in the cell.

When the diffusion is neglected, the cell performance is improved, resulting in a reduced R_{wg} with a decrease in time constant as previously mentioned. When the gas flow rate is doubled or when the channel height is reduced to a half of the current value, then τ_{wg} decreases less than a half, although the transit time of the gas becomes 50% shorter. This seems to be caused by a relatively weak effect of diffusion, as the mass transfer by convection doubles due to the doubled flow velocity, while the mass transfer by diffusion is hardly affected. The transit time does not change, even if the cell diameter is doubled for a given gas flow rate for unit cell area. However, there is a decrease in the time constant, which can also be explained by the same reason. According to Eq. (12), the gas conversion impedance is inversely proportional to the gas flow rate; however, R_{wg} becomes less than one-half by doubling the gas flow rate. This over-decreasing can also be explained by the relatively weak effect of the diffusion by doubling the gas flow velocity. For the same reason, R_{wg} is decreased by halving the channel height or by doubling the cell diameter.

With a 50 K decrease in temperature from 1023 K, there appears a small decrease of about 5–6% in R_{wg} as shown by (f) in Fig. 8. Most part of the decrease can be explained by the fact that the gas conversion impedance is proportional to the

Table 2
Equivalent circuit parameters for the parametric study of Figs. 10–12

Case	a	b	c	d	e
Equivalent circuit in Fig. 2	(a)	(a)	(b)	(b)	(b)
R_{cell} ($\Omega\,cm^2$)	0.5	1.0	–	–	–
R_i ($\Omega\,cm^2$)	–	–	0.5	0.25	0.25
R_r ($\Omega\,cm^2$)	–	–	0	0	0.1
C_d (F/cm^2)	–	–	0	0	0.16
R_e ($\Omega\,cm^2$)	–	–	12.5	10.0	10.0
R_s ($\Omega\,cm^2$)	–	–	0	0.25	0.15

temperature, as dictated by Eq. (12), though R_{wg} is affected by a decrease in the diffusion coefficients with decreased temperature. While the time constant increases about 4% by the decreased temperature as shown by (f) in Fig. 9, most of this increase can be also explained by Eq. (11). As the total pressure increased twice, R_{wg} does not change, and τ_{wg} is doubled as shown in Figs. 8 and 9. This can be verified via Eqs. (11) and (12), since the partial pressures become twice by doubling the pressure, simultaneously resulting in the halved volume flow rate.

3.4. Influence of local cell equivalent circuit parameters on total cell impedance

To examine the correlation between the local impedance and the total cell impedance, a simulation has been carried out for a variety of equivalent circuit parameters as shown in Table 2. The results for fuel utilization of 70 and 80% under the reference conditions are shown in Figs. 10 and 11.

In every case except case e, the normalized impedance on the high-frequency edge agrees with the local cell impedance. In case e, considering the complex impedance of an RC parallel circuit with the characteristic frequency of 10 Hz, the Cole–Cole plot looks as if a summation of the two semicircle impedances with characteristic frequencies are 10 and 0.4 Hz. In this case, the normalized whole-cell impedance on the high-frequency edge agrees with the local impedance on the high-frequency edge. It is indicated that the local impedance directly appears as the total cell impedance, when it is a frequency-depending complex impedance at much higher frequency than the characteristic frequency of the gas-conversion impedance. It was also suggested that the total impedance of the cell appears as the convolution of the local impedance and the gas conversion impedance.

When the local cell resistance R_{cell} increases from $0.5\,\Omega\,cm^2$ of the reference value to $1.0\,\Omega\,cm^2$, the semicircle of the Cole–Cole plot only parallel moves by $0.5\,\Omega\,cm^2$. However, the size of the impedance semicircle increases in all cases, when the electronic conductance is introduced using the equivalent circuit of Fig. 2b for the local impedance. The increase in the impedance is greater for 80% fuel utilization than for 70% utilization. Such increase in the impedance may be related to the increase in the effective fuel utilization induced by the current leak due to the electronic conductance. Therefore, the simulation for the effective fuel utilization U_{eff}, which is defined using the total reaction current instead of the total load current in Eq. (10), was carried out, and the parameter fitting to the simulation results using the equivalent circuit in Fig. 7b was performed. As a result, R_{wg} and τ_{wg} are shown against the effective fuel utilization U_{eff} in Figs. 12 and 13. Most of the plots in both figures are overlapping with each other, which indicate that the whole-cell gas-conversion impedance (R_{wg} and τ_{wg}) for a fixed effective fuel utilization scarcely depends on the local impedance.

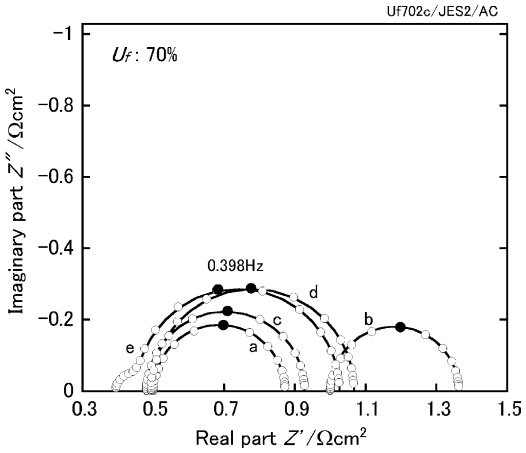

Fig. 10. Cole–Cole plots at 70% fuel utilization for various cases (a, b, c, d, e) of local-impedance parameters as shown in Table 2. Open and closed symbols: simulation results; Solid line: fitting by an equivalent circuit with an RC parallel circuit as shown in Fig. 7b. Closed symbol shows the point of the frequency value noted in the figure.

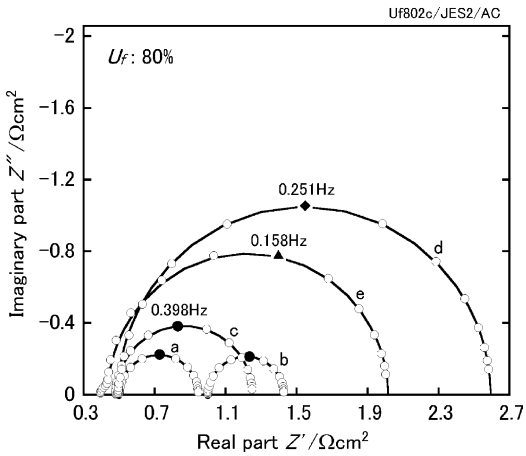

Fig. 11. Cole–Cole plots at 80% fuel utilization for various cases (a, b, c, d, e) of local-impedance parameters as shown in Table 2. Open and closed symbols: simulation results; Solid line: fitting by an equivalent circuit with an RC parallel circuit as shown in Fig. 7b. Closed symbol shows the point of the frequency value noted in the figure.

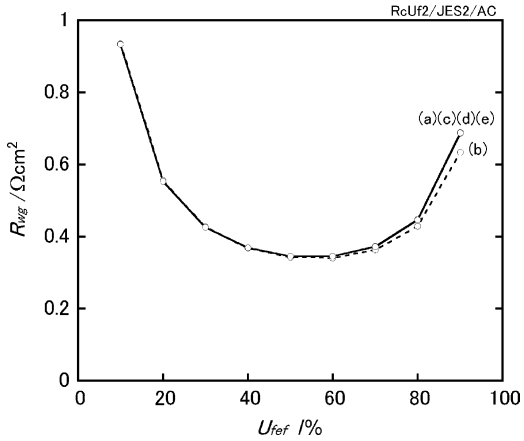

Fig. 12. R_{wg} vs. effective fuel utilization for the various local-impedance parameters as shown in Table 2 as cases a, b, c, d and e.

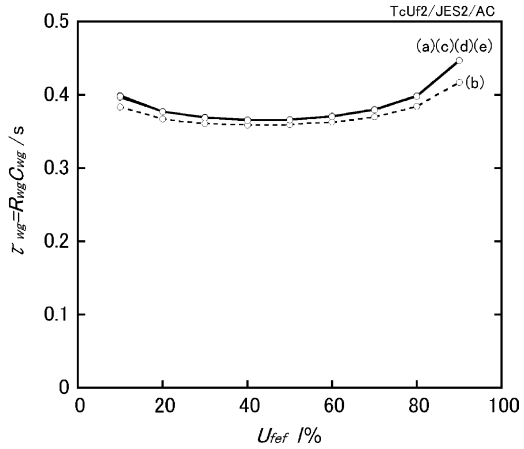

Fig. 13. τ_{wg} vs. effective fuel utilization for the various local-impedance parameters as shown in Table 2 as cases a, b, c, d and e.

4. Conclusions

A numerical simulation method which links the local impedance with the total cell impedance at power generation has been proposed. The simulation of the simple cases under experimental conditions is carried out to obtain the total cell impedance by changing parameters, such as ac frequency, fuel utilization, gas flow rate, etc. The following results have been found:

(1) The Cole–Cole plot for the total cell impedance shows a capacitive semicircle, even if a pure resistance is assumed as the local impedance, due to the gas conversion impedance which describes the change in the electromotive force by the kinetic current through the gas conversion due to the reaction. The high-frequency edge in the Cole–Cole plot agrees with the assumed local impedance.
(2) The whole-cell gas-conversion impedance is dependent on the fuel utilization, supplied gas flow rate, cell dimension, etc. It becomes larger as the fuel utilization approaches zero or 100% and has minimum value for the intermediate values of the fuel utilization. The whole-cell gas-conversion impedance is roughly inversely proportional to the supplied gas flow rate, being affected by the diffusion in the flow direction.
(3) The whole-cell gas-conversion impedance can be well expressed by an RC parallel circuit. Its time constant is roughly equal to the transit time of the fuel gas through the cell, being affected by the diffusion in the flow direction. It weakly depends on the fuel utilization, but considerably increases as the fuel utilization approaches either zero or 100%
(4) In an SOFC cell using electrolyte with electronic conductance, it is necessary to evaluate the whole-cell gas-conversion impedance using the effective fuel utilization considering the current leak due to the electronic conduction. The whole-cell gas-conversion impedance for a given effective fuel utilization weakly depends on the local cell impedance.

From the simulation results it is suggested that the total impedance of the cell appears as the convolution of the local impedance and the gas conversion impedance.

Acknowledgements

This study is carried out as a part of the “Evaluation of generating performance of SOFC, in R&D on the solid-oxide electrolyte fuel cell” project supported by Ministry of Economy, Trade and Industry.

Appendix A. Discussion on the parameter $\mathfrak{R}$

The three-dimensional molar-transport equation for a species M when no spatial species production is given as follows [15]:

$$\frac{\partial c_{\mathrm{M}}}{\partial t} + \nabla(c_{\mathrm{M}}\vec{v}) = \nabla(cD_{\mathrm{M}}\nabla x_{\mathrm{M}}). \tag{A.1}$$

where c_{M} the molar density (mol/cm^3), c the total molar density (mol/cm^3), $\vec{v}$ the molar average flow velocity vector (cm/s), D_{M} the diffusion coefficient (cm^2/s), x_{M} the mole fraction.

When axial symmetry and constant molar density are assumed, Eq. (A.1) can be described as follows:

$$\frac{\partial x_{\mathrm{M}}}{\partial t} + \frac{1}{r}\frac{\partial}{\partial r}(rv_{\mathrm{r}}x_{\mathrm{M}}) + \frac{\partial v_z x_{\mathrm{M}}}{\partial z} - \frac{1}{r}\frac{\partial}{\partial r}\left(rD_{\mathrm{M}}\frac{\partial x_{\mathrm{M}}}{\partial r}\right) - \frac{\partial}{\partial z}D_{\mathrm{M}}\frac{\partial x_{\mathrm{M}}}{\partial z} = 0 \tag{A.2}$$

To compare the distribution of the mole fraction between that in the z direction and that in the r direction, we neglect the r-direction diffusion term and the z-direction convection in the above equation and assume a steady state for simplic-

ity. Using continuity equation, the previous equation can be normalized as follows:

$$\mathfrak{R}\frac{\partial x_{\mathrm{M}}}{\partial \xi} - \frac{\partial^2 x_{\mathrm{M}}}{\partial \zeta^2} = 0 \tag{A.3}$$

where

$$\xi = \frac{r}{r_{\mathrm{o}}} \tag{A.4}$$

$$\zeta = \frac{z}{h} \tag{A.5}$$

$$\mathfrak{R} = \frac{\nu_{\mathrm{ro}} h^2}{r_{\mathrm{o}} D_{\mathrm{M}}} \tag{A.6}$$

where r_{o} is the outlet radius of cell; ν_{ro} the radial molar average flow velocity at cell outlet; h the height of flow channel.

By integrating the Eq. (A.3) for the cell volume, the following equation is obtained:

$$\int_0^1 (x_{\mathrm{M},\zeta=1} - x_{\mathrm{M},\zeta=0})\,\mathrm{d}\xi = \bar{\mathfrak{R}}\int_0^1\int_0^1 (x_{\mathrm{M},\xi=1} - x_{\mathrm{M},\xi=0})\mathrm{d}\zeta\,\mathrm{d}\zeta \tag{A.7}$$

where $\bar{\mathfrak{R}}$ is the mean value of $\mathfrak{R}$.

The Eq. (A.7) indicates that the difference of the mole fraction between $\zeta = 0$ (electrode surface) and $\zeta = 1$ (separator surface) is $\bar{\mathfrak{R}}$ times the difference between $\xi = 0$ (inlet) and $\xi = 1$ (outlet) as the average values. That is, the lateral change of the mole fraction in the channel is evaluated to be roughly $\mathfrak{R}$ times the longitudinal change at steady state.

References

[1] M.C. Williams, in: H. Yokogawa, S.C. Singhal (Eds.), Proceedings Series of The Electrochemical Society of the Solid Oxide Fuel Cells VII, PV 2001-16, Pennington, NJ, 2001, p. 3.

[2] G. Lequeux, in: H. Yokogawa, S.C. Singhal (Eds.), Proceedings of the Series of the Electrochemical Society of the Solid Oxide Fuel Cells VII, PV 2001-16, Pennington, NJ, 2001, p. 14.

[3] A. Muller, H Schichlein, M. Feuerstein, A. Weber, K. Krugel, E. Ivers-Tiffee, in: U. Stimming, S.C. Singhal (Eds.), Proceedings of the Electrochemical Society of the Solid Oxide Fuel Cells VI, PV99-19, Pennington, NJ, 1999, p. 925.

[4] R. Ihringer, S. Rambert, L. Constantin, J. Vanherle, in: H. Yokogawa, S.C. Singhal (Eds.), Proceedings Series of the Electrochemical Society of the Solid Oxide Fuel Cells VII, PV 2001-16, Pennington, NJ, 2001, p. 1002.

[5] J. Akikusa, T. Yamada, K. Adachi, K. Hoshino, T. Ishihara, Y. Takita, in: H. Yokogawa, S.C. Singhal (Eds.), Proceedings of the Electrochemical Society of the Solid Oxide Fuel Cells VII, PV 2001-16, Pennington, NJ, 2001, p. 159.

[6] T. Kato, K. Nozaki, A. Negishi, K. Kato, A. Monma, Y. Kaga, S. Nagata, K. Takano, T. Inagaki, H. Yoshida, K. Hosoi, K. Hoshino, T. Akbay, J. Akikusa, Impedance analysis of a disk type SOFC using doped lanthanum gallate under power generation, J. Power Sources, in press.

[7] A. Simrnova, K. Ellwood, G. Crosbie, J. Electrochem. Soc. 148 (6) (2001) A610–A615.

[8] M. Mogensen, T. Lindegaard, in: S.C. Singhal, H. Iwahara (Eds.), Proceedings Series of the Electrochemical Society of the Solid Oxide Fuel Cells, PV 93-4, Pennington, NJ, 1993, p. 484.

[9] B. van Hassel, B. Boukamp, A. Burggraaf, Solid State Ion. 48 (1991) 39–154, 155–171.

[10] R. Chiba, T. Ishii, in: M. Dokiya, O. Yamamoto, H. Tagawa, S.C. Singhal (Eds.), Proceedings Series of the Electrochemical Society of the Solid Oxide Fuel Cells IV, PV 95-1, Pennington, NJ, 1995, p. 482.

[11] A. Weber, A. Muller, D. Herbstrirt, E. Ivers-Tiffee, in: H. Yokogawa, S.C. Singhal (Eds.), Proceedings Series of the Electrochemical Society of the Solid Oxide Fuel Cells VII, PV 2001-16, Pennington, NJ, 2001, p. 952.

[12] F. Boulenouar, Y. Yashiro, M. Oishi, A. Kaimai, Y. Nigara, T. Kawada, J. Mizusaki, in: H. Yokogawa, S.C. Singhal (Eds.), Proceedings Series of the Electrochemical Society of the Solid Oxide Fuel Cells VII, PV 2001-16, Pennington, NJ, 2001, pp. 959–768.

[13] R.B. Bird, W.E. Stewart, E.N. Lightfoot, Transport Phenomena, Wiley, New York, 1960, p. 510.

[14] S. Primdahl, M. Mogensen, in: U. Stimming, S.C. Singhal, H. Tagawa, W. Lehnert (Eds.), Proceedings Series of the Electrochemical Society of the Solid Oxide Fuel Cells V, PV97-40, Pennington, NJ, 1997, p. 530.

[15] R.B. Bird, W.E. Stewart, E.N. Lightfoot, Transport Phenomena, Wiley, New York, 1960, p. 557.